PUBLISHED VERSION

Yu, Yang; Addai-Mensah, Jonas; Losic, Dusan,
Functionalized diatom silica microparticles for removal of mercury ions, Science and Technology of Advanced Materials, 2012; 13(1):015008-1-015008-11

© 2012 National Institute for Materials Science

PERMISSIONS

http://iopscience.iop.org/1468-6996/page/Copyright%20&%20permissions

Copyright & permissions

STAM's assignment of copyright form allows authors and their institutions to reproduce, distribute and communicate the **published version** of their article to the public. Under this agreement STAM authors may:

- post the published version of their article on their own personal website, on their employer's website/repository and on free public servers in their subject area;
- share print or electronic copies of their article with colleagues;
- use all or part of their article and abstract in personal compilations or other scholarly publications of their own work;
- use their article within their employer's institution or company for educational or research purposes, including use in course packs;
- make oral presentation of their article (all or part) and include a summary and/or highlights of it in papers distributed at such presentations or in conference proceedings.

Third parties have the same rights to reuse articles in STAM as described in the Creative Commons Attribution-NonCommercial-ShareAlike 3.0 license. These open access rights allow third-party users to copy, distribute and display the published version of articles in STAM, and create derivative works, subject to appropriate attribution and non-commercial exploitation.

24th April 2013

http://hdl.handle.net/2440/74890

IOP Publishing Science and Technology of Advanced Materials
Sci. Technol. Adv. Mater. **13** (2012) 015008 (11pp) doi:10.1088/1468-6996/13/1/015008

Functionalized diatom silica microparticles for removal of mercury ions

Yang Yu[1], **Jonas Addai-Mensah**[1] **and Dusan Losic**[1,2]

[1] Ian Wark Research Institute, University of South Australia, Mawson Lakes, SA 5095, Australia
[2] School of Chemical Engineering, The University of Adelaide, Adelaide, SA 5005, Australia

E-mail: dusan.losic@adelaide.edu.au

Received 7 August 2011
Accepted for publication 15 December 2011
Published 9 February 2012
Online at stacks.iop.org/STAM/13/015008

Abstract
Diatom silica microparticles were chemically modified with self-assembled monolayers of 3-mercaptopropyl-trimethoxysilane (MPTMS), 3-aminopropyl-trimethoxysilane (APTES) and n-(2-aminoethyl)-3-aminopropyl-trimethoxysilane (AEAPTMS), and their application for the adsorption of mercury ions (Hg(II)) is demonstrated. Fourier transform infrared spectroscopy and x-ray photoelectron spectroscopy analyses revealed that the functional groups (–SH or $–NH_2$) were successfully grafted onto the diatom silica surface. The kinetics and efficiency of Hg(II) adsorption were markedly improved by the chemical functionalization of diatom microparticles. The relationship among the type of functional groups, pH and adsorption efficiency of mercury ions was established. The Hg(II) adsorption reached equilibrium within 60 min with maximum adsorption capacities of 185.2, 131.7 and 169.5 mg g^{-1} for particles functionalized with MPTMS, APTES and AEAPTMS, respectively. The adsorption behavior followed a pseudo-second-order reaction model and Langmuirian isotherm. These results show that mercapto- or amino-functionalized diatom microparticles are promising natural, cost-effective and environmentally benign adsorbents suitable for the removal of mercury ions from aqueous solutions.

Keywords: diatoms, diatom silica, organosilane modifications, 3-mercaptopropyl-trimethoxysilane (MPTMS), mercury adsorption

1. Introduction

The fabrication of microscale materials with three-dimensional (3D) morphology and well-defined nanoscale features presents one of the biggest challenges in material science and nanotechnology. Nature, on the other hand, has developed a wide variety of highly sophisticated biomineralization processes to create solid structures with complex 3D morphology and hierarchical organization with nanoscale precision [1]. Diatoms, single-cell photosynthetic algae having an extraordinary 3D porous structure with micro- to nanoscale dimensions of their silica shells (frustules), are recognized as an outstanding example of nature-designed nanomaterials [2, 3]. Their distinct pore structures with unique mechanical, transport and photonic properties, moderate surface area and good biocompatibility made this biomaterial highly attractive for many applications, including photonics, sensing, biosensing, filtration, adsorption, microfluidics, catalysis, drug delivery and nanofabrication [3–5]. Diatom silica material is available from two sources, which include diatom cell cultures (small quantities) and diatomaceous earth mineral (DE, fossilized diatoms) in large quantities. Hence, it can be considered as an inexpensive biomaterial with nanoscale dimensions offering great perspectives for the development of new materials with advanced properties. Considerable research efforts have been devoted to modifying diatom silica structure into technologically more suitable functional materials such as inorganic oxides (MgO, TiO_2, zeolites), metals (Au) and polymers (polyaniline) [3–7]. In

 © 2012 National Institute for Materials Science Printed in the UK

our previous work, we showed that characteristic optical, catalytic and magnetic properties can be generated by the replication or structural and surface modification of diatom architecture with titania, gold or magnetic nanoparticles and used for diverse applications including molecular separation, catalysis and drug delivery [5, 8–13].

Mercury is recognized as one of the most harmful pollutants in the environment, because of its high toxicity, volatility and bioaccumulation. There are many sources of mercury pollution including natural processes such as volcanoes and flooding of river basins, industrial activity such as gaseous emissions of fossil fuel combustion, and industrial processes including chloralkali production, paint, pulp, fertilizer, pharmaceutical, rubber and paper industries, oil refineries and municipal solid waste treatment [14–16]. Commonly accepted methods for the removal of mercury from wastewater include sulfide and chelate precipitation, iron and aluminum coagulation, ion exchange, reverse osmosis, membrane filtration, electrodeposition, activated carbon adsorption, bioadsorption and photoreduction [17–19]. Among them, the adsorption using solid porous materials as adsorbents is considered as the most reliable, simple, efficient and cost-effective method. Numerous synthetic and natural adsorbents have been explored, including activated carbon, polymer resins, chitosan, starch, zeolite, clays, perlite, fly ash and synthetic mesoporous silica (MCM-41 and SBA-15) [20–22]. However, since commercially activated carbons and synthetic mesoporous materials are expensive or their production involves the use of toxic materials, the search for alternative and cheaper natural sorbents is a particularly attractive option.

For efficient mercury removal from water, porous adsorbents should have good chemical affinity to both inorganic and organic mercury, high adsorption speed and adsorption efficiency for low and high concentrations, high surface area, high mechanical strength, good thermal stability and low cost. Diatom silica in the form of porous microparticles from natural mineral, which retains diatoms' skeletal (frustules) structures with distinctive shapes and intricate mesoporosity, has been recognized as a superior and inexpensive adsorbent of heavy metals from water [5, 6]. It is an inexpensive (∼$200 per ton), chemically inert, biocompatible and environmentally friendly material, particularly suitable for environmental applications. A number of studies were performed to investigate the potential of DE as an absorbent for removing radionuclides, heavy metal ions (e.g. Pb(II), Zn(II), Cu(II), Cd(II) and Hg(II)) and textile dyes from wastewater [22–24]. While these studies have demonstrated a promising potential of DE for wastewater treatment, most of them used raw DE material, which is not optimized for specific applications. DE has a moderate surface area (20–100 $m^2\,g^{-1}$) and excellent porosity. Its surface chemistry is based on hydroxyl groups including single silanol groups (–SiOH), geminal silanol groups ($–Si(OH)_2$) and –Si–O–Si bridges, which have a limited adsorption capacity for specific metal ions such as Hg(II). The importance of having specific metal-binding functional groups (e.g. –SH) at the DE surface was recognized by Fowler *et al*, who functionalized an $(NH_4)_2HF_2$-pretreated DE surface with 3-mercaptopropyl-trimethoxysilane (MPTMS) and vinyltriethoxysilane (VTES) using a sol–gel procedure [25]. While the adsorption capacity of Hg(II) was improved in comparison with that of untreated DE, the results were not impressive, showing that only 3% of –SH sites on the functionalized DE surface were accessible to Hg(II) species [25]. This low efficiency can be explained by the oxidation of –SH groups or extensive unwanted organosilane polymerization on the DE surface. Hence, further studies are necessary to improve the functionalization of DE and provide a high density of active functional groups.

In this work, we explored the surface functionalization of diatom microparticles with self-assembled monolayers of selected organosilanes containing mercapto (–SH), amino ($–NH_2$), and ethylenediamino groups ($–NH–(CH_2)_2–NH_2$), aiming to demonstrate the improved adsorption properties of functionalized DE for the removal of Hg(II) ions from aqueous solutions. Our proposed approach, showing the typical structure of diatom microparticles and scheme of attached organosilane molecules, is presented in figure 1. We have studied the performance of organosilane-modified diatom particles for the adsorption capacity, efficiency toward Hg(II) ions, dependence of functional groups, contact time, initial metal ion concentration and pH. Mercuric chloride ($HgCl_2$) was used as the source of mercury ions (Hg(II)), as chloride ions are almost ubiquitous in natural and industrial waters and among the inorganic mercury complexes.

2. Experimental section

2.1. Materials

DE samples (white rocks, ∼2 cm in size) were provided by Mount Sylvia Pty Ltd (Queensland, Australia). They were mechanically crushed, pulverized, sieved (20 μm sieve), washed with Milli-Q water and dried [12], yielding fine (<20 μm) diatom particles. Mercury (II) chloride was supplied by Merck and toluene by Chem Supply (Australia). Organosilanes, including MPTMS, 3-aminopropyl-trimethoxysilane (APTES) and n-(2-aminoethyl)-3-aminopropyl-trimethoxysilane (AEAPTMS) were purchased from Sigma Aldrich (Australia). High-purity Milli-Q water (specific conductivity <0.5 $\mu S\,cm^{-1}$, surface tension 72.8 $mN\,m^{-1}$ and pH = 5.6 at 20 °C) was used for the preparation of all the aqueous solutions.

2.2. Surface modification of diatom microparticles

Diatom particles modified with organosilanes (MPTMS, APTES or AEAPTMS) were prepared by a standard silanization procedure used for the deposition of organosilane monolayers on mesoporous substrates [26]. Briefly, 5 g of diatom particles was suspended in 150 ml of toluene in a three-necked 500 ml round-bottomed flask, which was fitted with a thermometer, a reflux condenser and a N_2 gas tube and maintained under a dry N_2 atmosphere. Milli-Q water (1.6 ml) was then added into the mixture and stirred for 2 h at ambient temperature to allow the water to disperse through the diatom

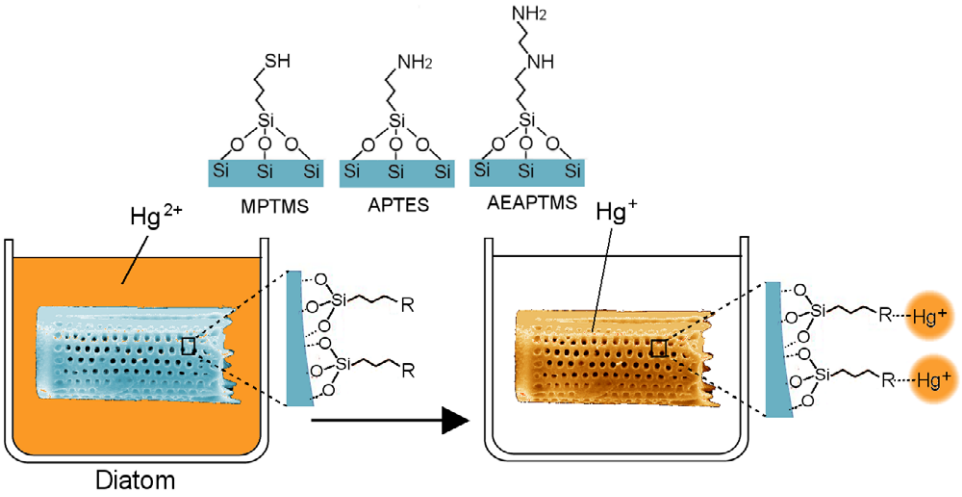

Figure 1. Surface modification of diatom microparticle for removal of mercury ions: SEM images of diatom structure and schemes of organosilane molecules covalently attached on diatom silica surface.

particles and make a fully hydroxylated silica surface. Then, 8.5 ml of organosilane (MPTMS, APTES or AEAPTMS) was added into the mixture, which was taken to reflux for 6 h at 60 °C. After that, the mixture was cooled and washed with toluene, 2-propanol and Milli-Q water 3 times. The samples modified with MPTMS, APTES or AEAPTMS were dried in a vacuum desiccator for 3 days.

2.3. Characterizations

Scanning electron microscopy (SEM, XL-30, Philips) was used to observe the morphology of diatoms before and after modifications.

The size distribution of diatom microparticles in water solution (1% w/v) was determined using the Malvern Mastersizer X, Malvern (UK). The zeta potentials were measured using the Nano-ZS Zetasizer in the electrophoretic light-scattering mode (Malvern Instruments Ltd, Worcestershire, UK) using diluted particle suspensions. We prepared 0.01 wt% suspensions by adding 0.25 g of dry pristine or organosilane-modified (MPTMS, APTES or AEAPTMS) diatom particles to 50 ml of a 10^{-3} M KNO_3 solution followed by magnetically stirring the suspensions for 20 min. The suspensions were then allowed to stand for 5 min and the colloidal particles ($<5\,\mu$m in size) in the supernatant were siphoned off for the zeta potential measurement in the pH range of 2–11.

Fourier transform infrared spectroscopy (FTIR) analysis of diatom particles was used to determine functional groups on their surface after modification. FTIR spectra were recorded with a Nicolet Magna-IR 750 spectrometer. A KBr pellet was prepared using a 1/100 proportion of diatom particles/KBr. For each spectrum, 128 scans were recorded at 4 cm^{-1} resolution, in the range of 4000–400 cm^{-1} in transmittance mode.

X-ray photoelectron spectroscopy (XPS) analysis was performed using an AXIS Ultra DLD spectrometer (Kratos Analytical Ltd) equipped with a monochromatic Al Kα source (1486.6 eV). Elements present were identified from survey spectra and high-resolution spectra, which were collected at 160 and 40 eV, respectively. Data were recorded in the VAMAS format and processed using the CasaXPS software package.

X-ray powder diffraction (XRD, Panalytical PW 3040) was used to characterize the crystallographic structure of diatom samples. X-ray fluorescence spectroscopy (XRF, Siemens SRS3000) and inductively coupled plasma mass spectrometry (ICP-MS, Perkin Elmer Optima 9000) analyses gave the elemental composition in terms of the oxide components of the samples and solution metal concentration.

Thermogravimetric analysis (TGA) was carried out using a Hi-Res Modulated TAG 2950 analyzer at a heating rate of 10 °C min^{-1} from 30 to 800 °C in a nitrogen gas flow.

The specific surface area (Brunauer–Emmett–Teller, BET analysis) of diatom samples was measured using a Micromeritics ASAP 2000 system.

2.4. Adsorption experiments

Adsorption isotherm experiments were carried out by varying the initial Hg(II) concentration from 1 to 400 mg l^{-1} to investigate the adsorption behavior of diatom particles modified with MPTMS, APTES or AEAPTMS. Standard solutions of Hg(II) were prepared by diluting of 400 mg l^{-1} Hg(II) ($HgCl_2$ in solution) with Milli-Q water. Then, 0.01 g of adsorbent was dispersed in 40 ml of Hg(II) solution. The mixture was magnetically stirred for 60 min to ensure equilibrium. The residual particle suspensions were filtered through a 0.45 μm membrane and the filtered solutions were analyzed for Hg(II) concentration using ICP-MS (Perkin Elmer Elan 9000). The effects of pH, contact time and initial Hg(II) concentration on the Hg(II) adsorption kinetics and isotherms were studied and all the experiments were replicated 3 times. Hg(II) adsorption capacity q (mg g^{-1}) and efficiency were calculated using the following equations [9]

$$q = \frac{(C_0 - C)V}{W}, \tag{1}$$

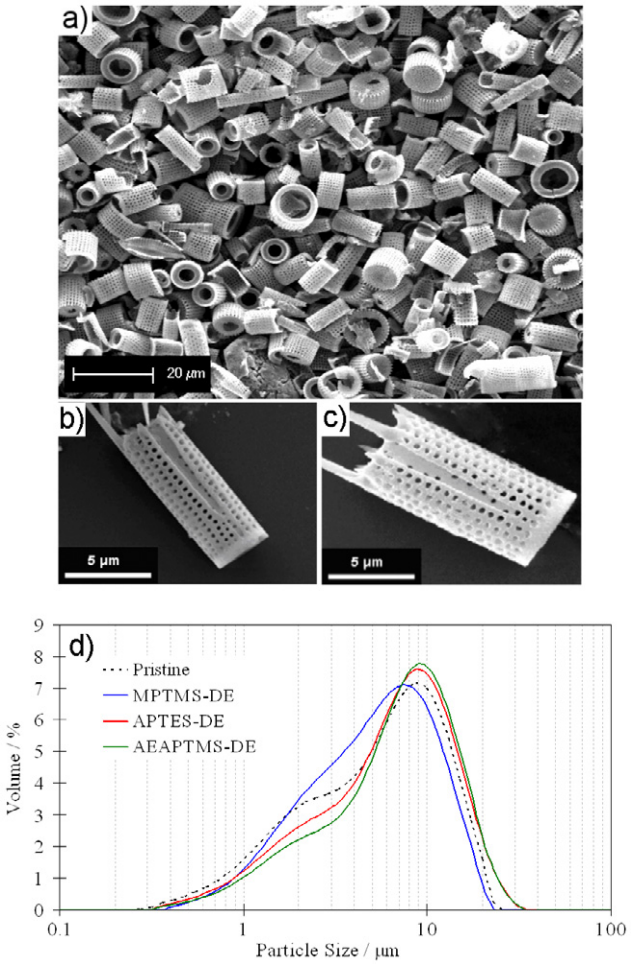

Figure 2. (a) SEM image of diatom particles from DE material used in this work; (b, c) SEM images of single diatom particles before and after surface modification with MPTMS-DE. (c) Particle size distribution of pristine diatoms and diatoms modified with MPTMS, APTES or AEAPTMS.

$$\text{Adsorption efficiency} = \frac{(C_0 - C)}{C_0} \times 100\%, \qquad (2)$$

where C_0 and C are the initial and equilibrium concentrations of Hg(II) (mg l^{-1}), respectively, V is the volume of solution (l) and W is the dry mass of adsorbent (g).

3. Results and discussion

3.1. Structural and chemical characterization of pristine and modified diatom microparticles

Figure 2 presents SEM images of the typical morphological structure of the diatom microparticles (frustules) used in this work, showing their perforated cylindrical shell with an opening at one end [12, 13]. Regularly spaced rows of pores of ∼300–500 nm diameters are located along the frustule shell wall (figure 2(b)). SEM images of diatoms modified with MPTMS, APTES or AEAPTMS confirmed that their morphologies and pore structures are the same as in the pristine diatoms (figure 2(c)). The 10th, 50th and 90th percentile particle sizes of the pristine diatom

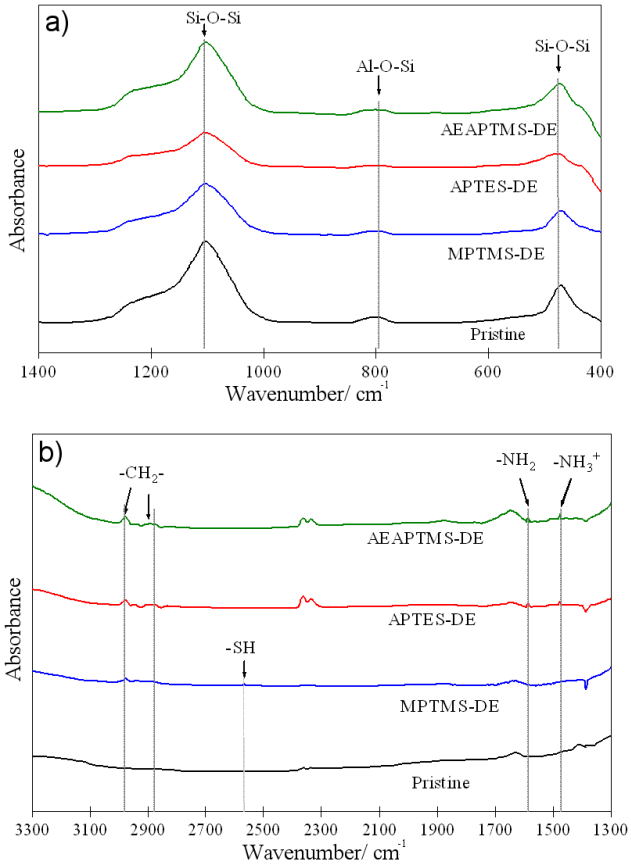

Figure 3. FTIR spectra of pristine diatoms and diatoms modified with MPTMS, APTES or AEAPTMS.

sample were 1.2, 5.5 and 12.7 μm, respectively (figure 2(d)), indicating that major diatom particles are whole frustule structures with minor fractures and aggregations. Again, no significant change of particle size distribution was observed in the modified diatoms (MPTMS-DE, APTES-DE and AEAPTMS-DE), confirming the formation of an ultrathin layer of organosilanes on the diatom's surface without aggregations. The BET surface area of pristine diatom microparticles was determined as $20.3 \pm 1.2\ m^2\ g^{-1}$, which is a moderate surface area for their proposed application in the adsorption of metal ions. The average pore diameter and pore volume of the pristine diatom particles were 12.4 nm and $0.052\ ml\ g^{-1}$, respectively. The BET specific surface area (∼$19.3\ m^2\ g^{-1}$), pore diameter (∼11.5 nm) and volume ($0.049\ ml\ g^{-1}$) of organosilane-modified diatom particles were similar to those of the pristine diatoms.

XRD analysis showed that the diatom microparticles mostly consist of amorphous silica with a trace amount of crystalline quartz, which is consistent with our previous studies [12, 13]. XRF analysis revealed that SiO_2 (∼90.2%) was the main oxide component in pristine diatoms with impurities such as Al_2O_3 (∼2.3%), Fe_2O_3 (∼0.8%), Mn, Mg and Ca as trace elements. A similar composition, but with a noticeable increase in C, S or N concentration was deduced from the XRF analysis of organosilane-modified samples.

Figure 3 shows the infrared absorption spectra of the pristine and organosilane-modified diatoms (MPTMS-DE,

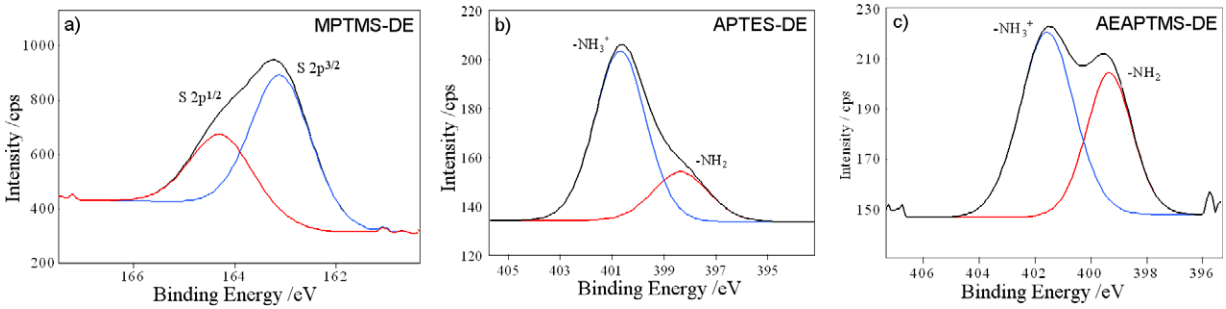

Figure 4. XPS spectra: (a) S 2p for MPTMS-DE, (b) N 1s for APTES-DE and (c) N 1s for AEAPTMS-DE samples.

Table 1. Atomic composition of the studied diatom particles determined from XPS analysis.

Sample	Atomic composition (%)				
	Si	O	C	S	N
Pristine DE	17.4	56.1	23.4	0	0
MPTMS	19.0	49.5	26.7	3.1	0
APTES-DE	18.4	48.2	28.6	0	3.1
AEAPTMS-DE	18.8	49.9	24.1	0	3.3

APTES-DE and AEAPTMS-DE). The vibrations observed at 468.3 and 1101.1 cm^{-1} correspond to asymmetric stretching modes of Si–O–Si bonds whilst the Al–O–Si stretching vibration is indicated at 800.8 cm^{-1} for both the pristine and organosilane-modified samples [27, 28]. Additional peaks at 1476.8, 1585.1, 2942.9, 2871.7 and 2566.8 cm^{-1} are observed in the MPTMS-DE, APTES-DE and AEAPTMS-DE samples. The vibrations at 2942.9 and 2871.7 cm^{-1} are associated with the asymmetric and symmetric stretching modes of the $–CH_2–$ moiety, respectively, which is directly related to the carbon chain of organosilane molecules [29, 30]. In the spectra of MPTMS-DE, the –SH stretching vibration occurs at about 2566.8 cm^{-1} and is associated with the functional group of the adsorbed MPTMS [29]. The scissor vibration of the $–NH_2$ terminal group (1585.1 cm^{-1}) and the deformation mode of the $–NH_3^+$ group (1476.8 cm^{-1}) are observed in the spectra of APTES-DE and AEAPTMS-DE samples. Both these modes are associated with the $–NH_2$ groups from APTES or AEAPTMS organosilanes [31]. These FTIR results clearly indicate the presence of –SH or $–NH_2$ functional groups on the diatom surface originating from MPTMS, APTES or AEAPTMS.

The XPS analyses of the elemental surface compositions of pristine and MPTMS-DE, APTES-DE and AEAPTMS-DE particles confirmed changes in the atomic concentrations of Si, C, N and S as a result of the modification process (figure 4 and table 1). The 23.4% C concentration in the pristine diatoms is due to the surface contamination. The increase in carbon concentration from 23.4 to 26.7, 28.6 and 24.1% in functionalized diatoms may correspond to the introduction of carbon chains from the MPTMS, APTES and AEAPTMS organosilanes, respectively, to the diatom surface [32, 33]. The surface functionalization by organosilanes was confirmed by high-resolution XPS measurements. The increase in the atomic concentration of sulfur from 0 to 3.1% in the MPTMS-modified sample indicates a successful surface functionalization with –SH groups [32]. The S 2p XPS signal (figure 4(a)) appears only in the MPTMS-treated sample, at around 163.18 eV with two peaks S $2p^{3/2}$ at 163.07 eV and S $2p^{1/2}$ at 164.25 eV), which can be attributed to the reduced sulfur (–SH) in the MPTMS mercapto group [34]. The N 1s peak (figures 4(b) and (c)) is only present in the APTES-DE and AEAPTMS-DE samples and the atomic concentration of nitrogen increases to 3.1 and 3.3%, respectively. The N ls peak was decomposed into two components: one at about 399.2 eV was attributed to the $–NH_2$ group and the other component at about 401.7 eV indicated the presence of protonated amines ($–NH_3^+$) [31, 32]. These XPS results confirm that the diatom silica surface is covered with –SH or $–NH_2$ groups from covalently attached MPTMS, APTES or AEAPTMS molecules.

TGA analyses provide further supporting evidence of the grafting of MPTMS, APTES and AEAPTMS onto the diatom surface. The TGA and derivative weight loss curves of the pristine and organosilane-modified diatom microparticles are presented in figures 5(a) and (b). The weight loss below 120 °C is due to the removal of physisorbed water whilst the weight reduction at 120–300 °C can be assigned to the expulsion of chemisorbed water [35]. The weight reduction at 400–800 °C may be associated with the dehydroxylation of the silica surface of diatoms. The main weight change in the temperature range of 300–400 °C was only observed in the organosilane-modified diatom particles, which can be ascribed to the oxidation and decomposition of the mercaptopropyl groups or aminopropyl groups coupled on the surface of diatom particles [36, 37]. The broad exothermic weight loss of organosilane-modified diatom particles in the range of 400 and 600 °C may be due to a combination of decomposition of strongly tethered organosilanes and the dehydration of silanol groups on the diatom surface [35–37].

The surface coverage of organosilanes can be estimated from the weight change between 300 and 600 °C (after subtracting the weight change of pristine diatom particles) using the following equation [38]:

$$S_N = \frac{\Delta W\% \times N_A}{EMW \times SSA_{BET}} \times 10^{-20} \text{ (number nm}^{-2}\text{)} \quad (3)$$

Here, S_N is the number of $–(CH_2)_3SH$, $–(CH_2)_3NH_2$ and $–(CH_2)_3NH(CH_2)_2NH_2$ groups per nm^2, $\Delta W\%$

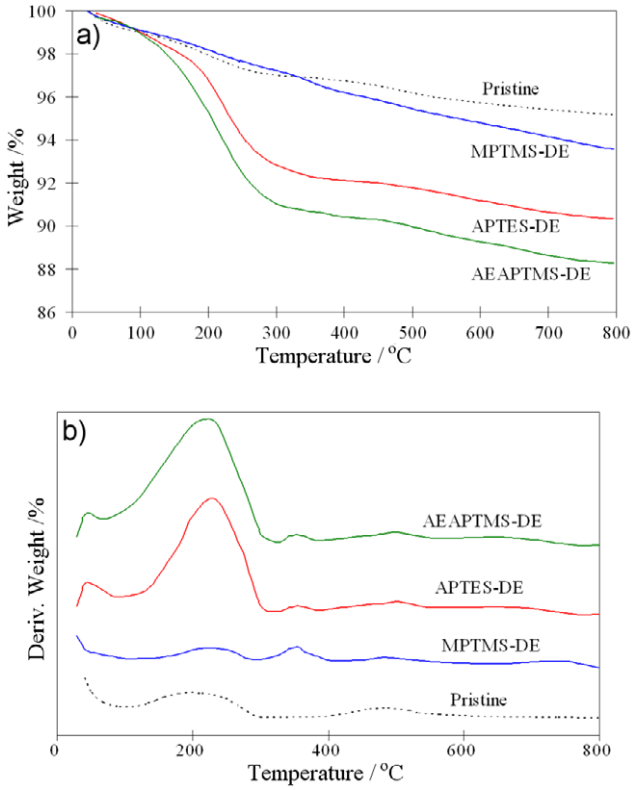

Figure 5. (a) TGA curves and (b) derivative weight-loss curves of pristine diatoms and diatoms modified with MPTMS, APTES or AEAPTMS.

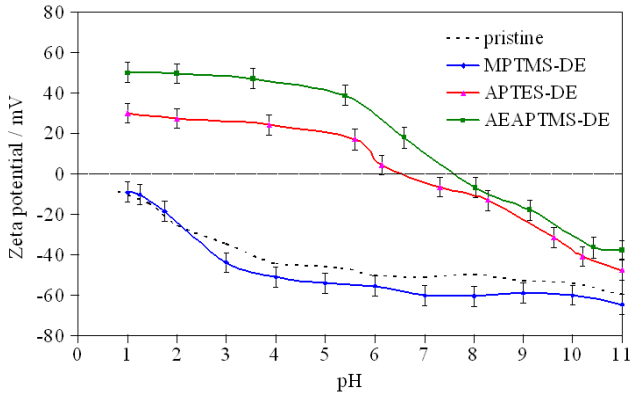

Figure 6. Zeta potential of pristine diatoms and diatoms modified with MPTMS, APTES or AEAPTMS as a function of pH in 10^{-3} M KNO_3 solution (pH was decreased from 11 to 2).

represents the difference in weight after silanization (%), N_A is Avogadro's number, EMW is the effective molar weight of the attached organosilane groups (g mol^{-1}), and SSA_{BET} is the BET specific surface area (m^2 g^{-1}). The densities of respective organosilane groups attached to the MPTMS/APTES/AEAPTMS-DE surfaces were calculated as 2.87, 2.55 and 2.48 nm^{-2} from the above equation, in agreement with the reported data [39].

The zeta potential of pristine diatom particles was negative in the pH range from 2 to 11, and its magnitude increased monotonically with increasing pH (figure 6). An isoelectric point (iep) close to pH = 2 is indicated, which

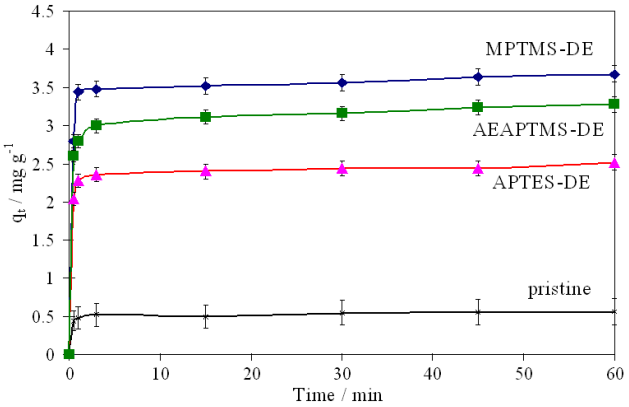

Figure 7. Adsorption capacity of pristine diatoms and diatoms modified with MPTMS, APTES or AEAPTMS at pH = 6 and initial Hg(II) concentration of 1 mg l^{-1}.

is quite similar to that of amorphous SiO_2 particles [40]. The zeta potential of MPTMS-DE particles did not change significantly in comparison with that of the pristine diatoms, despite the acidic nature of –SH groups form a negatively charged conjugate base on the diatom surface [41]. In diatoms modified with APTES or AEAPTMS, the zeta potentials shifted to more positive values due to the presence of protonated amines ($-NH_3^+$). As a result, isoelectric points (ieps) of pH 6.6 and 7.5 were observed for APTES and AEAPTMS-DE particles, respectively, in agreement with literature reports [41].

3.2. Adsorption studies of Hg(II)

The effectiveness of diatoms modified with MPTMS, APTES or AEAPTMS for Hg(II) extraction was investigated by comparing their adsorption capacity with that of the pristine diatoms (figure 7). The maximum adsorption capacity of pristine diatoms was 0.56 mg g^{-1} at pH = 6. This adsorption results from the interaction of positively charged Hg^{2+} ions with the negatively charged surface of diatom silica covered with hydroxy groups [42]. The adsorption capacities of diatoms modified with MPTMS, APTES or AEAPTMS were considerably higher at 3.68, 2.52 and 3.28 mg g^{-1}, respectively. These results reveal the enhanced adsorption capacity and confirm the strong affinity between the mercapto, amino and ethylenediamino groups on the diatom surface and Hg(II) species in solution [43].

The nature of hydrolyzable metal species present in solution varies significantly with pH and concentration of solubilized multivalent metal ion such as Hg(II), so it is expected that the pH affects the adsorption capacity of Hg(II). To understand how the pH-mediated speciation affects the interfacial processes of interest, analysis of Hg(II) speciation was undertaken [44]. Diagram of Hg(II)–OH–Cl$^-$ species indicates the presence of various Hg(II) complexes in aqueous mercury chloride media at different pH and chlorine concentrations [44]. $HgCl_2$ is the predominant species in the solution at chloride concentration [Cl] = 10^{-5} M in the pH range of 1–5. The Hg(II) ions hydrolyze into HgOHCl and $Hg(OH)_2$ at pH > 5. These species will affect the adsorption

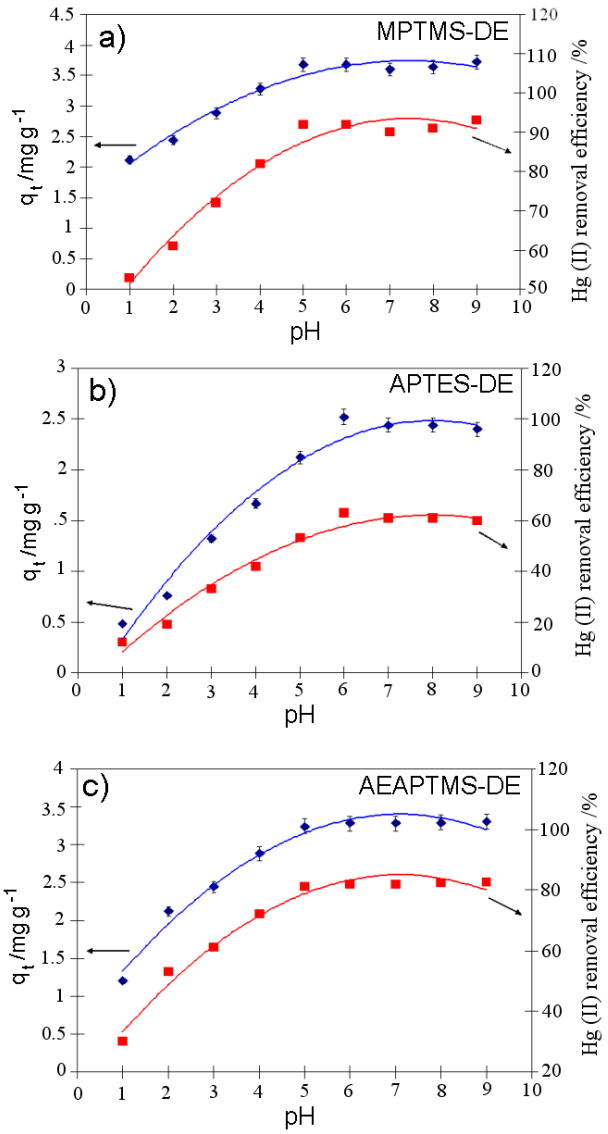

Figure 8. Effect of pH on the extraction of Hg(II) ions by (a) MPTMS-DE, (b) APTES-DE and (c) AEAPTMS-DE particles. Initial concentration of Hg(II) is 1 mg l^{-1} (60 min of contact time).

efficiency of Hg(II) in the solution upon interaction with protonated and deprotonated surface sites, which are affected by pH.

Figure 8 shows the pH dependence of the adsorption capacity and efficiency obtained for organosilane-modified diatoms in the pH range from 1 to 9. These graphs show that the adsorption capacity for Hg(II) was remarkably affected by pH, and the maximum adsorption by diatoms modified with MPTMS, APTES or AEAPTMS is observed in the pH range of 5–9. At pH < 5, decreasing trends in adsorption were observed as the $HgCl_2$ species became dominant in the solution [44]. These results reveal that the nature of Hg(II) species in solution at various pHs plays an important role in the interactions of the functional groups (–SH, –NH_2 and –NH–$(CH_2)_2$–NH_2) with the Hg(II) species, which determine the adsorption mechanisms. Hg(II) is known to have a strong affinity for halogens and ligands donating sulfur or nitrogen. At pH < 5, the decreasing trend in the adsorption of Hg(II) is due to the competition between the formation of mercury–sulfur or mercury–nitrogen bonds during the adsorption onto diatom particles modified with MPTMS-, APTES- or AEAPTMS and the stabilization of the chloro-complexes ($HgCl_2^0$) in solution [45, 46]. At pH > 5, where $Hg(OH)_2$ prevails, Hg(II) species can be effectively removed from solution by their specific interactions with the functional groups (–SH, –NH_2 and –NH–$(CH_2)_2$–NH_2) of MPTMS, APTES or AEAPTMS-modified diatoms [46].

At pH = 6, MPTMS-DE shows the highest adsorption efficiency (92.1%) of Hg(II) compared with APTES-DE and AEAPTMS-DE. This result indicates that sulfur-donating ligands (–SH) have a stronger capability of capturing Hg(II) than nitrogen-donating ligands (–NH_2 and –NH–$(CH_2)_2$–NH_2). The adsorption efficiency of AEAPTMS-DE (82.5%) is higher than that of APTES-DE (63.2%), which may be explained by the formation of the more stable diamino chloro–Hg(II) complex between the Hg(II) species and ethylenediamino groups originating from the AEAPTMS-DE surface [47]. Since all three adsorbents show the maximum adsorption efficiency for Hg(II) at pH = 6, this pH was selected for the other adsorption experiments and subsequent analyses.

3.3. Adsorption kinetics

The adsorption kinetics of diatom microparticles modified with MPTMS, APTES or AEAPTMS as a function of different initial concentrations of Hg(II) showed that adsorption occurred extremely rapidly at the beginning and reached equilibrium within 60 min (figures 9(a) and (c)). The equilibrium adsorption capacity (q_e) of all the three adsorbents increased significantly with increasing initial concentration of Hg(II) from 1 to 30 mg l^{-1}. This is due to the increase in initial concentration of Hg(II), providing a greater driving force for mass transfer and subsequent surface adsorption onto the diatom particles [48].

Both pseudo-first-order and pseudo-second-order empirical power law models may be used to evaluate the adsorption of Hg(II) onto the surface of diatoms modified with MPTMS, APTES or AEAPTMS. Empirical first- and second-order kinetic models are expressed with equation (4) for reaction exponents $n = 1$ and 2, respectively [49]

$$\frac{dq_t}{dt} = k_n(q_e - q_t)^n. \tag{4}$$

Here q_t (mg g^{-1}) and q_e (mg g^{-1}) represent adsorption capacity at contact time t and at equilibrium, respectively; k_1 and k_2 are the first- and second-order kinetic rate constants, respectively. Integrating equation (4) with the boundary conditions $t = 0$, $q_t = 0$ and $t = t$, $q_t = q_t$ to the linear form gives equations (5) and (6) for $n = 1$ and 2, respectively

$$\log(q_e - q_t) = \log q_e - \frac{k_1}{2.303}t, \tag{5}$$

$$\frac{t}{q_t} = \frac{1}{k_2 q_e^2} + \frac{t}{q_e}. \tag{6}$$

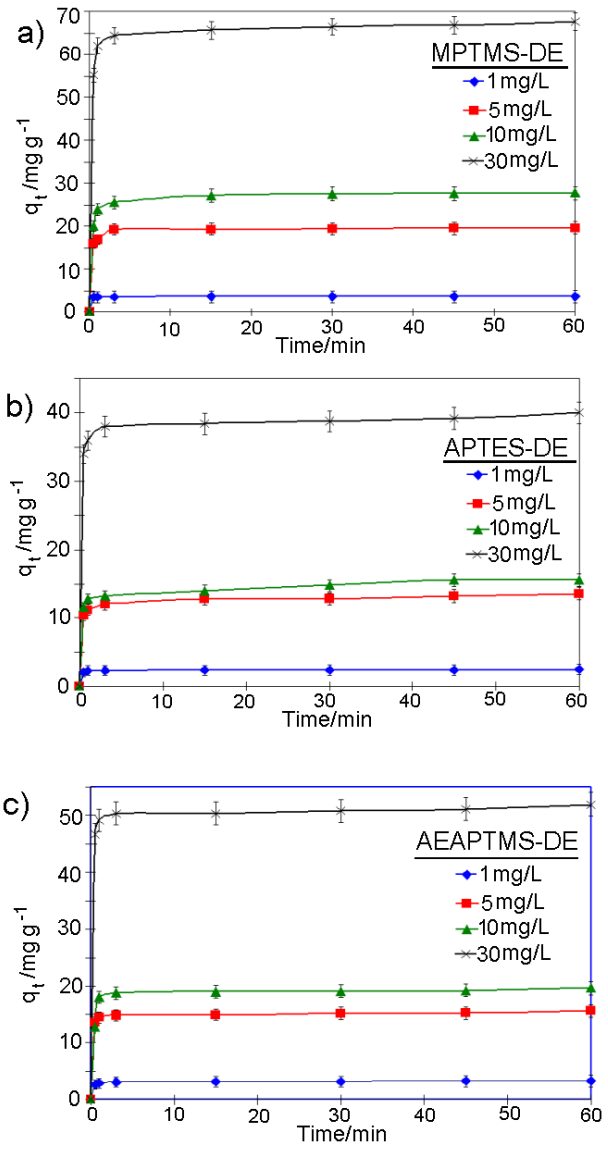

Figure 9. Effect of initial concentration on the adsorption capacities of diatom particles modified with (a) MPTMS, (b) APTES and (c) AEAPTMS.

The rate constants k_1 and k_2 may be determined from the slope of linear plots of $\log(q_e - q_t)$ versus t and the intercept of the linear plot of t/q_t versus t, respectively.

As can be seen from tables 2(a) and (b), the pseudo-second-order model fits the experimental data better than the pseudo-first-order model. The calculated q_e values (table 2(b)) from the pseudo-second-order model were also in good agreement with the experimental values q_e (exp). Thus, an empirical second-order model is suitable for the description of the adsorption kinetics of Hg(II) species onto modified diatom particles. The k_2 values (table 2(b)) indicate that the initial adsorption rate for organosilane-modified diatoms is much higher at a low Hg(II) concentration of 1 mg l^{-1} and the adsorption can reach equilibrium faster than in the solution with higher Hg(II) concentrations. The rate constant k_2 is larger for the mercapto-terminated (MPTMS-DE) than amino-terminated diatoms. This result may be explained by the stronger metal-binding capability of the –SH functional groups from the MPTMS-DE surface that allows the adsorption reaction to proceed faster. As for amino- and ethylenediamino-terminated adsorbents, the rate constant k_2 of AEAPTMS-DE is higher than that of APTES-DE, which may be attributed to the stronger affinity between the Hg(II) species and ethylenediamino groups from the AEAPTMS-DE surface.

3.4. Adsorption isotherms

Langmuir and Freundlich isotherms are commonly used for molecular adsorption at interfaces and for the prediction of equilibrium parameters [49]. The Langmuir model is based on the monolayer adsorption onto homogeneous active sites on adsorbents and can be expressed as [50]

$$\frac{C_{eq}}{q} = \frac{1}{q_{max} b} + \frac{C_{eq}}{q_{max}}. \tag{7}$$

Here, q_e is the adsorption capacity (mg g^{-1}), C_{eq} is Hg(II) concentration (mg l^{-1}) at equilibrium; b and q_{max} are the Langmuir constant (l mg^{-1}) and maximum adsorption capacity (mg g^{-1}) determined by the intercept and slope of the linear plot of C_{eq}/q versus C_{eq}, respectively.

The Freundlich isotherm is based on the adsorption onto a heterogeneous surface with uniform energy with no restriction to the formation of a monolayer. It may be expressed as [51]

$$\log q_e = \log K_f + \frac{1}{n} \log C_{eq}, \tag{8}$$

where K_f is the Freundlich adsorption constant (l mg^{-1}) and $1/n$ is the adsorption intensity (dimensionless). These parameters can be respectively calculated from the intercept and slope of the plot of $\log q_e$ versus $\log C_{eq}$.

From table 3, we can conclude that the regression coefficients R^2 are significantly higher for the Langmuir model ($R^2 = 0.99$–1.00) than for the Freundlich model ($R^2 = 0.89$–0.96), suggesting that the Langmuir adsorption isotherm is more suitable for describing the adsorption of Hg(II) onto MPTMS-DE, APTES-DE and AEAPTMS-DE (figure 10). The process may be assumed to occur at substantially homogeneous functional groups and binding sites on the surface of the adsorbents up to a monolayer coverage [47]. Compared with amino-terminated adsorbents (APTES-DE, AEAPTMS-DE), the –SH functionalized adsorbent MPTMS-DE shows the highest maximum adsorption capacity of 185.2 mg g^{-1} for Hg(II). The adsorption capacity for Hg(II) of MPTMS-DE is considerably higher than that of other thiol-DE-based materials (9.0–13.4 mg g^{-1}) prepared using the sol–gel process in air [25]. The maximum adsorbed amount of Hg(II) (0.926 mM g^{-1}) indicates that up to 95.6% of the thiol centers could bind the Hg(II) species, which is much higher than a previously reported value for MPTMS-DE (3%) [25]. This significant improvement is the result of a higher density of active –SH groups on the DE surface and can be explained by the preparation using a nonaqueous solvent (toluene) under nitrogen atmosphere. The grafting of organosilane layers of MPTMS in aqueous

Table 2. (a) Pseudo-first-order and (b) pseudo-second-order kinetic parameters of Hg(II) adsorption onto modified diatom microparticles.

Sample	C of Hg(II)	(a) Pseudo-first-order model		
	(mg ml^{-1})	k_1 (min^{-1})	q_e (cal) (mg g^{-1})	R^2
MPTMS-DE	1	0.129	0.36	0.62
	5	0.141	2.76	0.65
	10	0.177	5.79	0.83
	30	0.151	11.21	0.75
APTES-DE	1	0.132	0.50	0.71
	5	0.128	3.79	0.81
	10	0.165	5.09	0.88
	30	0.145	7.23	0.74
AEATMS-DE	1	0.139	0.77	0.81
	5	0.115	2.56	0.66
	10	0.132	3.66	0.66
	30	0.141	6.58	0.65

Sample	C of Hg(II)	q_e (exp)	(b) Pseudo-second-order model		
	(mg ml^{-1})		k_2 (g mg^{-1} min^{-1})	q_e (cal) (mg g^{-1})	R^2
MPTMS-DE	1	3.61	1.793	3.59	0.99
	5	19.60	0.313	19.61	1.00
	10	27.72	0.141	27.78	1.00
	30	67.61	0.064	67.56	0.99
APTES-DE	1	2.52	0.863	2.49	0.99
	5	13.60	0.136	13.49	0.99
	10	15.61	0.087	15.67	1.00
	30	40.01	0.086	39.83	0.99
AEAPTMS-DE	1	3.28	1.104	3.27	0.99
	5	15.62	0.224	15.50	1.00
	10	19.59	0.176	19.53	0.99
	30	52.00	0.093	51.81	0.99

Table 3. Langmuir and Freundlich isotherm parameters.

Sample	Langmuir model			Freundlich model		
	b (ml mg^{-1})	q_{max} (mg g^{-1})	R^2	K_f (ml mg^{-1})	n	R^2
MPTMS-DE	0.077	185.2	1.00	22.61	2.463	0.89
APTES-DE	0.029	131.6	0.99	6.651	1.817	0.95
AEAPTMS-DE	0.037	169.5	0.99	10.732	1.926	0.96

solution in air could lead to the formation of oxidized disulfide moieties and multilayer formation that could significantly decrease the density of active –SH groups. The adsorption capacity of functionalized DE materials reported in this study is relatively high compared with those of other low-cost adsorbents (20.6–89.1 mg g^{-1}) [24, 52–54], modified mesoporous-silica-based adsorbents (20.8–249.0 mg g^{-1}) [55–59] and modified activated carbon (67.8–121.6 mg g^{-1}) [21, 43, 60]. For instance, the kinetics of Hg(II) adsorption onto MPTMS-DE particles is considerably faster (>92.1% recovery in 15 min) and the equilibrium adsorption capacity (3.6–185.2 mg g^{-1}) is at least twice greater than those reported for MPTMS-modified zeolite particles in similar mercury adsorption studies [24].

It should be noted that although DE particles have much a lower BET specific surface area than the conventional

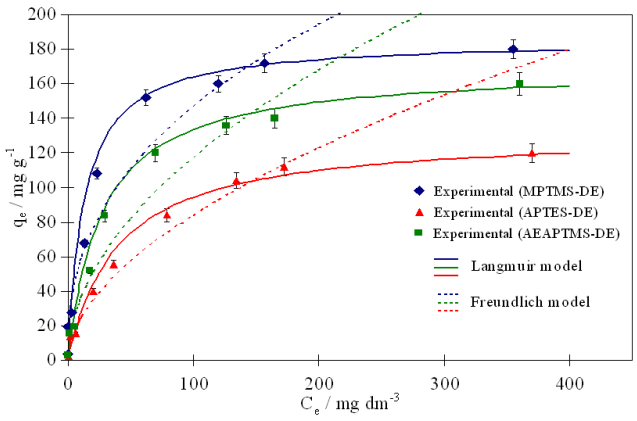

Figure 10. Adsorption isotherms of Hg(II) onto diatom particles modified with MPTMS, APTES or AEAPTMS.

Table 4. Comparison of adsorption capacities for Hg(II) of different nano- to mesoporous adsorbents.

Reference	Adsorbent	S_{BET}	Maximum adsorption capacity	
		($m^2\ g^{-1}$)	($mg\ g^{-1}$)	($mg\ m^{-2}$)
[25]	MPTMS-functionalized DE	9.0	9.0–13.4	1.0–1.5
[52]	Carbon aerogel	700.0	35.0	0.05
[24]	MPTMS-zeolite	–	89.1	–
[56]	1-furoyl thiourea urea-functionalized SBA-15	378.0	122.0	0.32
[57]	Ammonium-functionalized magnetic mesoporous silica	427.3	20.0	0.05
[58]	MPTMS-MCM-41	448.8	249.0	0.55
[59]	2-mercaptothiazoline-functionalized SBA-15	507.0	220.0	0.43
[59]	2-mercaptothiazoline-functionalized MCM-41	804.0	140.0	0.17
[21]	1-acylthiosemicarbazide-modified activated carbon	–	67.8	–
[60]	Hybrid ligand-modified activated carbon	650.0	121.6	0.19
[43]	APTES-activated carbon	650.0	97.5	0.15
This work	MPTMS-DE	19.3	185.2	9.6

synthetic mesoporous adsorbents, the maximum adsorption capacity for Hg(II) at an equal surface area ($9.6\ mg\ m^{-2}$) is significantly higher for modified DE than for modified mesoporous silica or activated carbon ($0.05–0.55\ mg\ m^{-2}$). A comparison of our results and previously reported data is presented in table 4. It suggests that the functionalized DE particles have superior adsorption efficiency for Hg(II) per unit surface area, which may be ascribed to superior organosilane grafting and increased density of accessible active sites on the DE surface. Studies are underway using natural water samples and industrial wastewaters containing several ion species to reveal more information on Hg(II) adsorption behavior, kinetics, adsorption isotherms and selectivity of functionalized diatom particles.

4. Conclusions

Surface modification of diatom particles with MPTMS, APTES and AEAPTMS was successfully carried out and their application as an effective adsorbent of Hg(II) was demonstrated. Diatom particles modified with mercapto groups (MPTMS-DE) show higher adsorption efficiency than diatoms modified with amino groups (APTES-DE and AEAPTMS-DE), confirming a stronger capability of sulfur-donating functional groups (–SH) for capturing Hg(II) ions. The adsorption capacity for Hg(II) was affected by pH in the solution and the maximum adsorption was observed in the pH range of 5–9. The Hg(II) adsorption reached equilibrium within 60 min, resulting in maximum adsorption capacities of 185.2, 131.7 and $169.5\ mg\ g^{-1}$ for MPTMS-DE, APTES-DE and AEAPTMS-DE, respectively. The organosilane-based diatom material is a promising adsorbent for the removal of Hg ions from aqueous solutions. The approach presented in this work can be used for designing diatom adsorbents of various metal ions.

Acknowledgment

The authors acknowledge the financial support by the Australian Research Council (ARC LP 0989229) and Mt Sylvia Pty Ltd.

References

[1] Sarikaya M, Tamerler C, Jen A K Y, Schulten K and Baneyx F 2003 *Nat. Mater.* **2** 577
[2] Hildebrand M 2008 *Chem. Rev.* **108** 4855
[3] Sumper M and Brunner E 2006 *Adv. Funct. Mater.* **16** 17
[4] Gordon R, Losic D, Tiffany M A, Nagy S S and Sterrenburg F A S 2009 *Trends Biotechnol.* **27** 116
[5] Losic D, Mitchell J G and Voelcker N H 2009 *Adv. Mater.* **21** 2947
[6] Lopez P J, Descles J, Allen A E and Bowler C 2005 *Curr. Opin. Biotechnol.* **16** 180
[7] Bao Z *et al* 2007 *Nature* **446** 172
[8] Losic D, Mitchell J G and Voelcker N H 2006 *New J. Chem.* **30** 908
[9] Losic D, Mitchell J G, Lal R and Voelcker N H 2007 *Adv. Funct. Mater.* **17** 2439
[10] Losic D, Triani G, Evans P J, Atanacio A, Mitchell J G and Voelcker N H 2006 *J. Mater. Chem.* **16** 4029
[11] Losic D, Yu Y, Aw M S, Simovic S, Thierry B and Addai-Mensah J 2010 *Chem. Commun.* **46** 6323
[12] Aw M S, Simovic S, Addai-Mensah J and Losic D 2011 *Nanomedicine* **6** 1159
[13] Yu Y, Addai-Mensah J and Losic D 2010 *Langmuir* **26** 14068
[14] Fitzgerald W F and Clarkson T W 1991 *Environ. Health Perspect.* **96** 159
[15] Boening D W 2000 *Chemosphere* **40** 1335
[16] Bodaly R A, St Louis V L, Paterson M J, Fudge R J, Hall B D, Rosenberg D M and Rudd J W 1997 *Met. Ions Biol. Syst.* **34** 259
[17] Bessbousse H, Rhlalou T, Verchère J F and Lebrun L 2008 *J. Membr. Sci.* **325** 997
[18] Veglio F and Beolchini F 1997 *Hydrometallurgy* **44** 301
[19] Miretzky P and Cirelli A F 2009 *J. Hazard. Mater.* **167** 10
[20] Budinova T, Petrov N, Parra J and Baloutzov V 2008 *J. Environ. Manag.* **88** 165
[21] Gao R *et al* 2009 *J. Hazard. Mater.* **172** 324
[22] Merrifield J D, Davids W G, MacRae J D and Amirbahman A 2004 *Water Res.* **38** 3132
[23] Ma X, Li Y, Ye Z, Yang L, Zhou L and Wang L 2011 *J. Hazard. Mater.* **185** 1348
[24] Zhang X Y, Wang Q C, Zhang S Q, Sun X J and Zhang Z S 2009 *J. Hazard. Mater.* **168** 1575
[25] Fowler C E, Buchber C, Lebeau B, Patarin J, Delacôte C and Walcarius A 2007 *Appl. Surf. Sci.* **253** 5485
[26] Feng X, Fryxell G E, Wang L Q, Kim A Y, Liu J and Kemner K M 1997 *Science* **276** 923
[27] Sheng G *et al* 2009 *Colloids Surf.* A **339** 159
[28] Huang J, Liu Y, Jin Q, Wang X and Yang J 2007 *J. Hazard. Mater.* **143** 541

[29] Liang X, Xu Y, Sun G, Wang L, Sun Y and Qin X 2009 *Colloid Surf. Physicochem. Eng. Aspect* **349** 61
[30] Finocchio E, Macis E, Raiteri R and Busca G 2007 *Langmuir* **23** 2505
[31] Maria Chong A S and Zhao X S 2003 *J. Phys. Chem.* B **107** 12650
[32] Briand E *et al* 2011 *Langmuir* **27** 678
[33] Yang S R and Kolbesen B O 2008 *Appl. Surf. Sci.* **255** 1726
[34] Hu M, Noda S, Okubo T, Yamaguchi Y and Komiyama H 2001 *Appl. Surf. Sci.* **181** 307
[35] Guan M, Liu W, Shao Y, Huang H and Zhang H 2009 *Microporous Mesoporous Mater.* **123** 193
[36] Kao H M, Shen T Y, Wu J D and Lee L P 2008 *Microporous Mesoporous Mater.* **110** 461
[37] Möller K, Kobler J and Bein T 2007 *J. Mater. Chem.* **17** 624
[38] Zhao X S, Lu G O, Whittaker A K, Millar G J and Zhu H Y 1997 *J. Phys. Chem.* B **101** 6525
[39] Moon J H, Kim J H, Kim K J, Kang T H, Kim B, Kim C H, Hahn J H and Park J W 1997 *Langmuir* **13** 4305
[40] Franks G V 2002 *J. Colloid Interface Sci.* **249** 44
[41] Kuo C H, Chang H Y, Liu C P, Lee S H, You Y W and Shyue J J 2011 Phys. Chem. *Chem. Phys.* **13** 3649
[42] Delacôte C, Gaslain F O M, Lebeau B and Walcarius A 2009 *Talanta* **79** 877
[43] Zhu J, Yang J and Deng B 2009 *J. Hazard. Mater.* **166** 866
[44] Baes C F and Mesmer R E 1976 *The Hydrolysis of Cations* (New York: Wiley)
[45] He Z, Traina S J and Weavers L K 2007 *Environ. Sci. Technol.* **41** 779
[46] Pearson R G 1988 *Inorg. Chem.* **27** 734
[47] Baba Y, Ohe K, Kawasaki Y and Kolev S D 2006 *Reactive Funct. Polym.* **66** 1158
[48] Al-Ghouti M A, Khraisheh M A M, Ahmad M N M and Allen S 2009 *J. Hazard. Mater.* **165** 589
[49] Ho Y S 2004 *Carbon* **42** 2115
[50] Kraus A, Jainae K, Unob F and Sukpirom N 2009 *J. Colloid Interface Sci.* **338** 359
[51] Freundlich H M F 1906 *J. Phys. Chem.* **57** 385
[52] Kadirvelu K, Goel J and Rajagopal C 2008 *J. Hazard. Mater.* **153** 502
[53] Meena A K, Kadirvelu K, Mishra G K, Rajagopal C and Nagar P N 2008 *J. Hazard. Mater.* **150** 604
[54] Ghassabzadeh H, Mohadespour A, Torab-Mostaedi M, Zaheri P, Maragheh M G and Taheri H 2010 *J. Hazard. Mater.* **177** 950
[55] Pérez-Quintanilla D, Del Hierro I, Fajardo M and Sierra I 2006 *Microporous Mesoporous Mater.* **89** 58
[56] Mureseanu M, Reiss A, Cioatera N, Trandafir I and Hulea V 2010 *J. Hazard. Mater.* **182** 197
[57] Liu J and Du X 2011 *J. Mater. Chem.* **21** 6981
[58] Idris S A, Harvey S R and Gibson L T 2011 *J. Hazard. Mater.* **193** 171
[59] Pérez-Quintanilla D, Hierro I D, Fajardo M and Sierra I 2006 *J. Hazard. Mater.* **134** 245
[60] Zhu J, Deng B, Yang J and Gang D 2009 *Carbon* **47** 2014